Space-time evolution and HBT analysis of relativistic heavy ion collisions in a chiral $SU(3) \times SU(3)$ model.

D. Zschiesche,[1] S. Schramm,[2] H. Stöcker,[1] and W. Greiner[1]

[1]*Institut für Theoretische Physik, Postfach 11 19 32, D-60054 Frankfurt am Main, Germany*

[2]*Argonne National Laboratory, 9700 S. Cass Avenue, Argonne IL 60439, USA*

Abstract

The space-time dynamics and pion-HBT radii in central heavy ion-collisions at CERN-SPS and BNL-RHIC are investigated within a hydrodynamic simulation. The dependence of the dynamics and the HBT-parameters on the EoS is studied with different parametrizations of a chiral SU(3) $\sigma - \omega$ model. The selfconsistent collective expansion includes the effects of effective hadron masses, generated by the nonstrange and strange scalar condensates. Different chiral EoS show different types of phase transitions and even a crossover. The influence of the order of the phase transition and of the latent heat on the space-time dynamics and pion-HBT radii is studied. A small latent heat, i.e. a weak first-order chiral phase transition, or a smooth crossover lead to distinctly different HBT predictions than a strong first order phase transition. A quantitative description of the data, both at SPS energies as well as at RHIC energies, appears difficult to achieve within the ideal hydrodynamic approach using the SU(3) chiral EoS. A strong first-order quasi-adiabatic chiral phase transition seems to be disfavored by the pion-HBT data from CERN-SPS and BNL-RHIC.

1. INTRODUCTION

General theoretical arguments [1] and lattice QCD simulations [2] predict the occurrence of a transition of strongly interacting matter to a state where chiral symmetry is (approximately) restored. Since Bose-Einstein correlations in multiparticle production processes [3] provide valuable information on the space-time dynamics of fundamental interactions [4], correlations of identical pions produced in high energy collisions of heavy ions may provide information on the characteristics of that phase transition (for a review on QGP signatures, see [5]). For recent reviews on this topic we refer to [6, 7].

In particular, a first order phase transition leads to a prolonged hadronization time as compared to a cross-over or a hadron gas with no symmetry restoration, and has been related to unusually large Hanbury-Brown–Twiss (HBT) radii [8, 9, 10]. The coexistence of hadrons and QGP reduces the "explosivity" of the high-density matter before hadronization, prolonging the emission duration of pions [8, 9, 10]. This phenomenon should then depend on the critical temperature T_c and the latent heat of the transition. Typically, calculations assuming a first-order phase transition are carried out with an equation of state (EoS) derived from matching the bag model with an ideal hadron gas model, for which the latent heat of the transition is large [9, 10]. Consequently, the predicted HBT radii were large.

Here, we consider also the case of a more weakly first-order transition with small latent heat and study the influence on the space time characteristics of the expansion and on the HBT radii. Furthermore, we perform explicit calculations for a smooth transition (crossover) at high temperatures, and discuss the resulting pion HBT radii. Such a scenario was considered in [10], however without explicit reference to chiral symmetry restoration and dynamical hadron masses.

To investigate the space-time dynamics and the influences of different types of phase transitions, hydrodynamic expansion with an EoS obtained from a chiral $SU(3)_L \times SU(3)_R\, \sigma - \omega$ model is considered. The equations of fluid dynamics describe the collective evolution of the system, while the chiral $SU(3) \times SU(3)$ model yields the underlying equation of state. Thus, as the hot and dense central region expands both in the longitudinal and transverse directions, the hadrons approach their vacuum masses. The initial excitation energy is converted into both, collective flow *and* massive hadrons. This purely hadronic model describes successfully nuclear matter ground state properties, finite nuclei and hadron masses in the

vacuum [17, 18]. Furthermore, it exhibits different kinds of high temperature transitions, depending on the set of parameters. Using the various equations of state in a hydrodynamic simulation should discriminate between the different phase transition scenarios. Since the model only contains hadronic degrees of freedom, we only test the influence of the chiral phase transition but not of the deconfinement phase transition. In any case, the main effect as far as collective expansion is concerned, is due to the difference in the latent heat for the transition, irrespective of its microscopic origin.

This article is organized as follows. In section 2 we present our model. In particular, in 2.1 we discuss ideal relativistic hydrodynamics, and in 2.2 we refer to our equations of state. Section 3 shows our main results for the space-time evolution and the pion HBT radii. We summarize and conclude in section 4. Throughout the manuscript, we employ natural units $c = \hbar = k_B = 1$.

2. MODEL DESCRIPTION

2.1. Scaling Hydrodynamics

Ideal Hydrodynamics is defined by (local) energy-momentum and net charge conservation [11],

$$\partial_\mu T^{\mu\nu} = 0 \quad , \quad \partial_\mu N_i^\mu = 0 \quad . \tag{1}$$

$T^{\mu\nu}$ denotes the energy-momentum tensor, and N_i^μ the four-current of the ith conserved charge. We will explicitly consider only one such conserved charge, the net baryon number. We implicitly assume that the local densities of all other charges which are conserved on strong-interaction time scales, e.g. strangeness, charm, and electric charge, vanish. The corresponding four-currents are therefore identically zero, cf. eq. (2), and the conservation equations are trivial.

For ideal fluids, the energy-momentum tensor and the net baryon current assume the simple form [11]

$$T^{\mu\nu} = (\epsilon + p)\, u^\mu u^\nu - p g^{\mu\nu} \quad , \quad N_B^\mu = \rho_B u^\mu \quad , \tag{2}$$

where ϵ, p, ρ_B are energy density, pressure, and net baryon density in the local rest frame of the fluid, which is defined by $N_B^\mu = (\rho_B, \vec{0})$. $g^{\mu\nu} = \mathrm{diag}(+,-,-,-)$ is the metric tensor, and $u^\mu = \gamma(1, \vec{v})$ the four-velocity of the fluid ($\vec{v}$ is the three-velocity and $\gamma = (1 - \vec{v}^2)^{-1/2}$

the Lorentz factor). The system of partial differential equations (1) is closed by choosing an equation of state (EoS) in the form $p = p(\epsilon, \rho_B)$, cf. below.

For simplicity, we assume cylindrically symmetric transverse expansion with a longitudinal scaling flow profile, $v_z = z/t$ [12]. This should be a reasonable first approximation for central collisions at high energy (such as at CERN-SPS and BNL-RHIC energies), and around midrapidity. A quantitative comparison to experimental data, which we postpone to a future publication, should however analyze the effects due to coupling of longitudinal and transverse flows around midrapidity. At least up to CERN-SPS energies, $\sqrt{s} \sim 20A$ GeV, such a coupling was shown to exist [13].

The hydrodynamic equations of motion are solved on a discretized space-time grid ($\Delta r_T = R_T/100 = 0.06$ fm, $\Delta\tau = 0.99\Delta r_T$) by employing the RHLLE algorithm as described and tested in [10, 15]. We have checked that the algorithm accurately conserves total energy and baryon number, and that profiles of rarefaction and shock waves are reproduced accurately for various initial conditions [14, 15, 16].

As already mentioned above, eqs. (2), we assume a perfect, i.e. non-dissipative, relativistic fluid. In principle, it is possible to calculate the transport coefficients from the Lagrangean of our model [17, 18]. (For example, various transport coefficients have been computed in the symmetry broken phase based on the assumption of an ideal gas of hadrons [19].) Also, dynamical simulations indicate that dissipation strongly affects the pion correlation functions at small relative momentum, and thus the deduced HBT radii [20]. Quantitative comparisons to experimental data should therefore account for dissipative effects. On the other hand, the purpose of this paper is to explore the effects from varying the latent heat and the order of the phase transition. In that vein, we can leave aside the great technical and principal difficulties related to a treatment of dissipation in dynamical simulations [21], and give an impression of the largest possible effects of varying the phase transition parameters that can be expected. This will also allow for a comparison to previous results for the pion HBT correlation functions, which employed ideal fluid dynamics with an EoS derived from the bag model [9, 10].

2.2. Equations of state from a chiral $SU(3) \times SU(3)$ model

To close the system of coupled equations of hydrodynamics, an equation of state (EoS) has to be specified. Lattice QCD predicts chiral symmetry restoration at a critical temperature of $T_c = 140 - 170$ MeV [2, 22] (for $\rho_B = 0$). We obtain the equation of state from a chiral $SU(3) \times SU(3)\sigma - \omega$ model that was discussed in detail in [17, 18]. We will briefly introduce the model here: consider a relativistic field theoretical model of baryons and mesons based on a nonlinear realization of chiral symmetry and broken scale invariance. The general form of the Lagrangean is:

$$\mathcal{L} = \mathcal{L}_{\rm kin} + \sum_{M=X,Y,V,\mathcal{A},u} \mathcal{L}_{\rm BM} + \mathcal{L}_{\rm vec} + \mathcal{L}_{\rm VP} - \mathcal{V}_0 - \mathcal{V}_{\rm SB}. \tag{3}$$

$\mathcal{L}_{\rm kin}$ is the kinetic energy term, $\mathcal{L}_{\rm BM}$ includes the interaction terms of the different baryons with the various spin-0 and spin-1 mesons. The baryon masses are generated by both, the nonstrange σ ($< q\bar{q} >$) and the strange ζ ($< s\bar{s} >$) scalar condensate. X,Y,V,A,u stand for scalar octet, scalar singlet, vector, axial vector and pseudoscalar mesons respectively. $\mathcal{L}_{\rm VP}$ contains the interaction terms of vector mesons with pseudoscalar mesons. $\mathcal{L}_{\rm vec}$ generates the masses of the spin-1 mesons through interactions with spin-0 mesons, and $\mathcal{V}_0$ gives the meson-meson interaction terms which induce the spontaneous breaking of chiral symmetry. It also includes a scale-invariance breaking logarithmic potential. Finally, $\mathcal{V}_{\rm SB}$ introduces an explicit symmetry breaking of the $\mathrm{U}(1)_A$, the $\mathrm{SU}(3)_V$, and the chiral symmetry. All these terms have been discussed in detail in [17, 18].

The hadronic matter properties at finite density and temperature are studied in the mean-field approximation, i.e. the meson field operators are replaced by their expectation values and the fermions are treated as quantum mechanical one-particle operators [23]. After performing these approximations, the Lagrangean (3) becomes

$$\begin{aligned}
\mathcal{L}_{BM} &= -\sum_i \overline{\psi_i}[g_{i\omega}\gamma_0\omega^0 + g_{i\phi}\gamma_0\phi^0 + m_i^*]\psi_i \\
\mathcal{L}_{vec} &= \frac{1}{2}m_\omega^2\frac{\chi^2}{\chi_0^2}\omega^2 + \frac{1}{2}m_\phi^2\frac{\chi^2}{\chi_0^2}\phi^2 + g_4^4(\omega^4 + 2\phi^4) \\
\mathcal{V}_0 &= \frac{1}{2}k_0\chi^2(\sigma^2+\zeta^2) - k_1(\sigma^2+\zeta^2)^2 - k_2(\frac{\sigma^4}{2}+\zeta^4) - k_3\chi\sigma^2\zeta \\
&+ k_4\chi^4 + \frac{1}{4}\chi^4\ln\frac{\chi^4}{\chi_0^4} - \frac{\delta}{3}\chi^4\ln\frac{\sigma^2\zeta}{\sigma_0^2\zeta_0}
\end{aligned}$$

$$\mathcal{V}_{SB} \;=\; \left(\frac{\chi}{\chi_0}\right)^2 \left[m_\pi^2 f_\pi \sigma + (\sqrt{2} m_K^2 f_K - \frac{1}{\sqrt{2}} m_\pi^2 f_\pi)\zeta\right],$$

with m_i the effective mass of the baryon i ($i = N, \Lambda, \Sigma, \Xi, \Delta, \Sigma^*, \Xi^*, \Omega$). σ and ζ correspond to the scalar condensates, ω and ϕ represent the iso-singlet non-strange and the strange vector field, respectively, and χ is the dilaton field, which can be viewed as representing the effects of the gluon condensate. In this work we will use the frozen glueball approximation, i.e. adopt the dilaton field as constant. In the current form of the model this makes sense, since the glueball field does not change strongly with temperature and density. In a forthcoming work we will investigate the consequences of a stronger coupling of the glueball field to the scalar fields.

The thermodynamical potential of the grand canonical ensemble Ω per volume V at a given chemical potential μ and temperature T can be written as:

$$\begin{aligned}
\frac{\Omega}{V} \;&=\; -\mathcal{L}_{vec} + \mathcal{V}_0 + \mathcal{V}_{SB} - \mathcal{V}_{vac} \\
&-\; \frac{1}{T}\sum_i \frac{\gamma_i}{(2\pi)^3} \int d^3k \left[\ln\left(1 + e^{-\frac{1}{T}[E_i^*(k) - \mu_i^*]}\right)\right] \\
&+\; \frac{1}{T}\sum_j \frac{\gamma_j}{(2\pi)^3} \int d^3k \left[\ln\left(1 - e^{-\frac{1}{T}[E_j^*(k) - \mu_j]}\right)\right]
\end{aligned}$$

The vacuum energy $\mathcal{V}_{vac}$ (the potential at $\rho = 0$) has been subtracted in order to get a vanishing total vacuum energy. γ_i denote the fermionic and γ_j the bosonic spin-isospin degeneracy factors. The single particle energies are $E_i^*(k) = \sqrt{k_i^2 + m_i^{*2}}$, with $m_i^* = m_i^*(\sigma, \zeta)$ (see [17, 18]). The effective baryonic chemical potentials read $\mu_i^* = \mu_i - g_{i\omega}\omega - g_{i\phi}\phi$ with $\mu_i = (n_q^i - n_{\bar{q}}^i)\mu_q + (n_s^i - n_{\bar{s}}^i)\mu_s$ and the mesonic chemical potentials read $\mu_j = (n_q^j - n_{\bar{q}}^j)\mu_q + (n_s^j - n_{\bar{s}}^j)\mu_s$. n_q^i, $n_{\bar{q}}^i$,n_s^i and $n_{\bar{s}}^i$ denote the number of consituent q, $\bar{q}$, s and $\bar{s}$ quarks in particle species i, respectively.

The mesonic fields are determined by extremizing $\frac{\Omega}{V}(\mu, T)$: The density of particle i can be calculated by differentiating Ω with respect to the corresponding chemical potential μ_i. This yields:

$$\rho_i = \gamma_i \int_0^\infty \frac{d^3k}{(2\pi)^3} \left[\frac{1}{\exp\left[(E_i^* - \mu_i^*)/T\right] \pm 1}\right]$$

The net density of particle species i is given by $\rho_i - \bar{\rho}_i$. The energy density and the pressure follow from the Gibbs–Duhem relation, $\epsilon = \Omega/V + TS + \mu_i \rho^i$ and $p = -\Omega/V$. The model shows a phase transition or a crossover around $T_c = 150$MeV. Since there are only hadronic

degrees of freedom in the model, this phase transition is of purely hadronic nature, i.e. the strong increase of the scalar density reduces the masses of the baryons, which in turn again increases the scalar density (compare e.g. to [24]).

The characteristics (e.g. the order, the latent heat) of the various phase transitions depend on the chosen parameters and on the considered degrees of freedom. We will use three different parameter sets, which differ in their treatment of the baryon resonances. This leads to different predictions concerning the behavior of hot hadronic matter. In parameter set CI the baryon decuplet is neglected, and the only degrees of freedom in the system are the members of the (anti)-baryon octet, the pseudoscalar meson nonet and the vector meson nonet. In parameter set CII and CIII we include the (anti)-baryon decuplet. This increases the number of degrees of freedom by 80. The parameter sets CII and CIII differ in the treatment of the strange spin-$\frac{3}{2}$ resonances. In parameter set CII an additional explicit symmetry breaking for the baryon resonances along the hypercharge direction, as desribed in [17] for the baryon octet, is included. This is neglected in parameter set CIII.

In figure 1 the resulting pressure and energy density are plotted as a function of temperature for vanishing chemical potential. The predicted behavior of the hot hadronic matter differs significantly for the different parameter sets. Parameter set CI exhibits a smooth crossover, while a first order phase transition is found for parameter set CII. Two first order phase transitions are found for parameter set CIII. This behavior is due to separate jumps in the non-strange and the strange condensate.

The resulting velocities of sound are shown in figure 2. The crossover EoS shows a decrease of c_s^2 around $\epsilon = 1\text{GeV/fm}^3$. This is due to the strong reduction of the baryonic masses around the phase transition region. However, because the latent heat is zero in the crossover case, c_s^2 remains finite. In contrast c_s^2 vanishes in the phase transition regions for CII and CIII (however, it is non-zero if $\mu_q, \mu_s > 0$). The latent heat for CII is $\Delta E_{II} \approx 600\text{MeV/fm}^3$, while it is $\Delta E_{III} \approx 850\text{MeV/fm}^3 + 920\text{MeV/fm}^3 = 1770\text{MeV/fm}^3$ for CIII (Both values are for $\mu_q = \mu_s = 0$). Between the two distinct first-order transitions in model III, c_s^2 is non-zero again. However, this happens in a very narrow interval of energy density, and plays no significant role in our analysis.

As can be seen from Fig 2 r.h.s., the occurence of a first order phase transition depends on the chemical potential. For small chemical potential, $\mu_q < 100\text{MeV}$, CIII shows two phase transitions due to the jump in the σ and the ζ field while CII exhibits one PT due

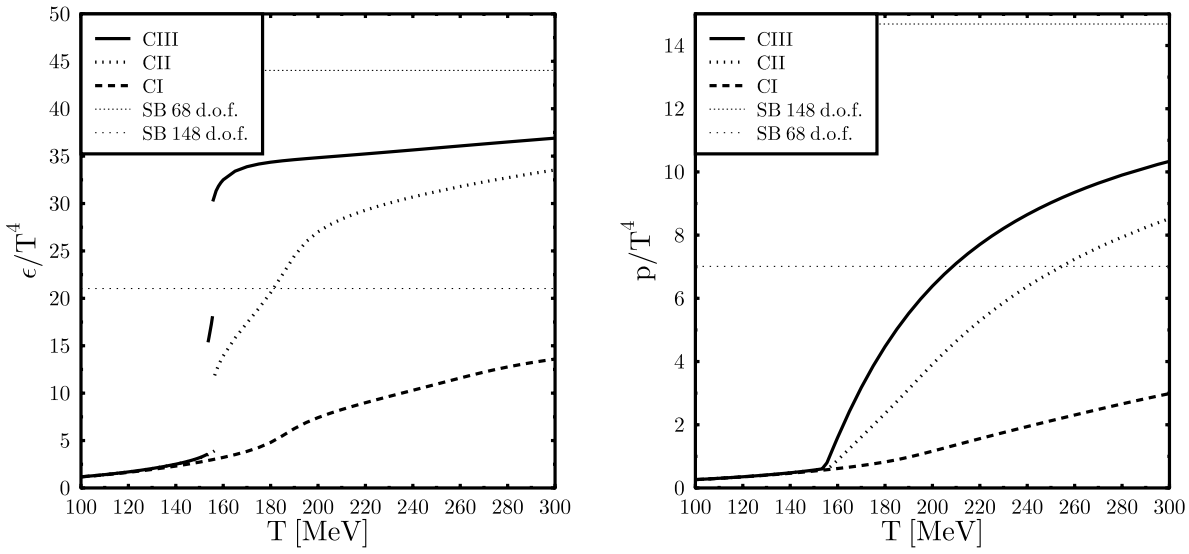

FIG. 1: ϵ/T^4 and p/T^4 for the three different parameter sets CI, CII, CIII at $\mu_q = \mu_s = 0$. Depending on the chosen parameters we observe a different phase transition behavior. For CI a smooth crossover occurs. In contrast CII leads to a jump in ϵ/T^4 at $T \approx 150$MeV and a discontinuity in the rise of P/T^4 with T. Finally, CIII even shows two discontinuities in ϵ/T^4. The horizontal lines correspond to the Stefan-Boltzmann limit with and without the (anti)-baryon decuplet.

to the jump in the σ-field. At higher chemical potentials, ($100\text{MeV} < \mu_\text{q} < 370\text{MeV}$) CIII shows a phase transition due to the jump in the ζ field only. Furthermore, since in the $SU(3)$-approach two chemical potentials (μ_q, μ_s) have to be considered, the condition $f_s \equiv \rho_s/\rho_B = 0$ does not hold for each phase in the mixed-phase region, but only for the *t*otal strangeness fraction. This leads to a slight change of the temperature in the mixed phase. For chemical potential $\mu_q > 370$MeV there is no phase transition for $f_s = 0$. The energy densities and entropy densities in the phase transition regions are specified in table I.

The effective thermodynamic potential for parameter set CII around the phase transition temperature T_c is depicted in figure 3. We observe that the effective thermodynamic potential varies very rapidly around T_c. The spinodal points, i.e. the temperatures at which the inflection points for the two minima appear, are only $2-3\%$ off T_c. This potential therefore varies substantially faster than that from the Gross-Neveu model or from the $SU(2)$ linear sigma model investigated in [25]. However, the variation of the potential around T_c ob-

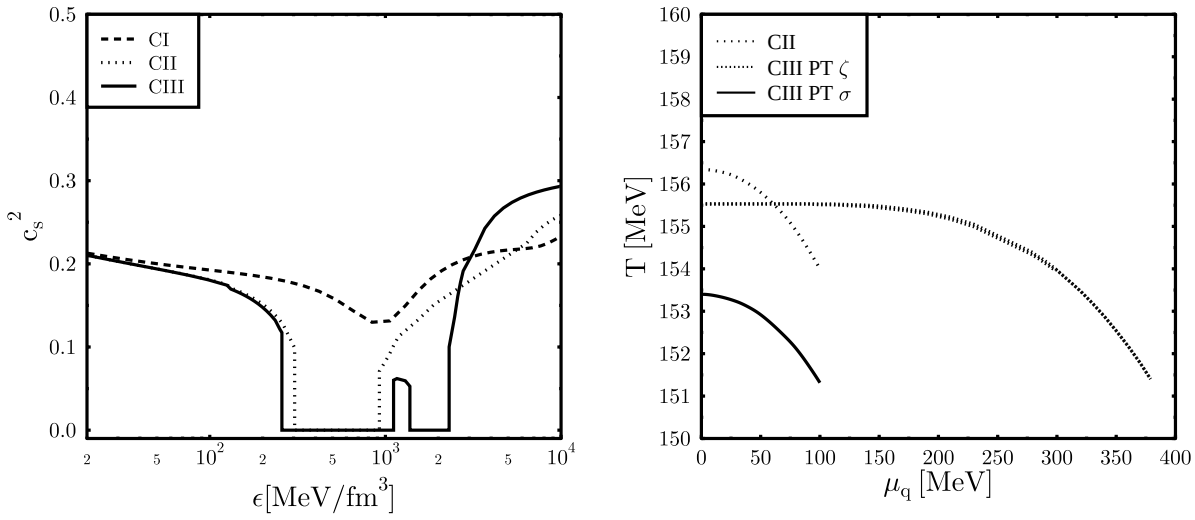

FIG. 2: Left: $c_s^2 \equiv \partial p/\partial\epsilon$ for three different equations of state at $\mu_q = \mu_s = 0$. Right: Phase diagram for the parameter sets CII and CIII for $f_s \equiv \rho_s/\rho_B = 0$. The two chemical potentials (μ_q, μ_s) of the system lead to a slight change of the temperature in the phase transition region.

	ϵ^-/ϵ_0	ϵ^+/ϵ_0	$s^-[fm^{-3}]$	$s^+[fm^{-3}]$	T_c[MeV]
CII	2.1	6.3	2.3	6.2	156.3
CIII - 1st PT	1.7	7.6	2.0	7.5	153.4
CIII - 2nd PT	9.4	15.7	9.3	15.2	155.5

TABLE I: Energy density and entropy density in the phase transition regions for CII,CIII, $\mu_q = \mu_s = 0$. The $(-), (+)$ signs stand for values below and above the phase transition, respectively. T_c denotes the phase transition temperature. $\epsilon_0 = 138.45$ MeV/fm^3 denotes the energy density of nuclear matter in the ground state.

tained from our model is in the same range as for the model used in [28], where the authors showed that such a fast variation of the effective potential around T_c might lead to explosive behavior via rapid spinodal decomposition (as opposed to an adiabatic phase transition). This questions the applicability of our approach of equilibrium hydrodynamics. However, as a first approximation, we study the effects dynamically, assuming that local equilibrium does hold, i.e. that the mean fields in fact assume the value of the global minimum of the potential, and that at the critical temperature two phases (corresponding to the two minima

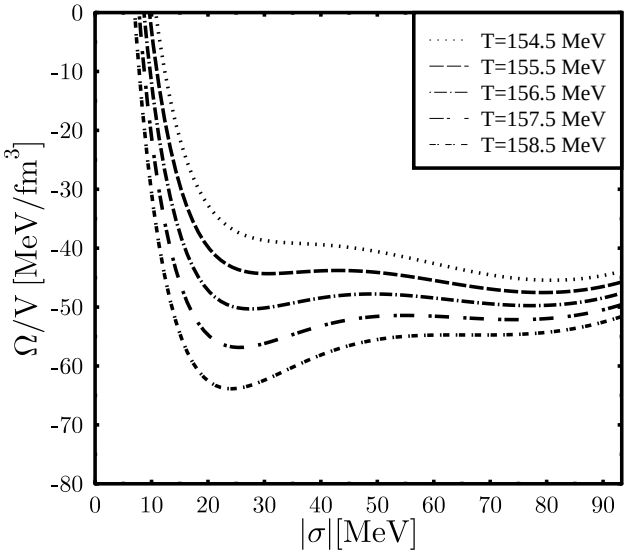

FIG. 3: Effective Potential $\Omega/V \equiv -p$ as a function of the scalar condensate σ around T_c. For parameter set CII and $\mu_q = \mu_s = 0$ (ζ has been chosen such as to maximize the pressure for given σ).

of the effective potential) coexist.

2.3. Initial Conditions

The initial conditions in scaling hydrodynamics are specified on a proper-time hyperbola $\tau = \tau_i$. On that space-like hypersurface one has to specify the entropy per net baryon and the net baryon rapidity density at midrapidity, dN_B/dy. A model with an MIT bag model equation of state [29] for the high temperature phase and an ideal hadron gas in the low-temperature region can reproduce both [14], the measured transverse energy at midrapidity, and the p_T-spectra of a variety of hadrons at $\sqrt{s} = 17.4A$ GeV (CERN-SPS energy), assuming the standard thermalization (proper) time $\tau_i = 1$ fm/c, and a specific entropy of $s/\rho_B = 45$ and a net baryon rapidity density $dN_B/dy = 80$. This value for s/ρ_B is also in good agreement with the measured relative abundances of hadrons [30]. The initial net baryon density follows as $\rho_B = 4.5\rho_0$. The corresponding values of ϵ_i, T, μ_q and μ_s (q- and s-quark chemical potential respectively) for the various chiral EoS are listed in table II.

		ϵ/ϵ_0	p/ϵ_0	T[MeV]	μ_q[MeV]	μ_s[MeV]
SPS	CI	49.2	10.5	256.0	236.2	133.0
	CII	40.2	6.6	197.0	241.3	58.6
	CIII	37.3	5.9	180.6	246.6	36.4
RHIC	CI	127.9	29.3	313.3	138.4	95.8
	CII	100.4	21.4	242.0	151.6	60.9
	CIII	93.7	22.0	230.0	154.6	53.0

TABLE II: Initial conditions for the three chiral EoS, corresponding to $s/\rho_B = 45$ and $dN_B/dy = 80$ for CERN-SPS energy and $s/\rho_B = 200$ and $dN_B/dy = 25$ for BNL-RHIC energy. $\epsilon_0 = 138.45$ MeV/fm^3 is the energy density of nuclear matter in the ground state. Here, ϵ and s/ρ_B denote the average values at midrapidity at the initial time τ_i, i.e. the mean of the respective transverse distribution. The other quantities have been computed from those average values for ϵ and s/ρ_B, using the corresponding EoS.

The initial net baryon density is independent of the underlying EoS because the continuity equation for the net baryon current in (1) does not involve the pressure p explicitly.

Due to the higher density at midrapidity, thermalization may be faster at BNL-RHIC energies – following [10] we assume $\tau_i = 0.6$ fm/c. Various microscopic models, e.g. PCM [31], RQMD [32], FRITIOF 7.02 [33], and HIJING/B [34], predict a net baryon rapidity density of $dN_B/dy \approx 20 - 35$ and specific entropy of $s/\rho_B \approx 150 - 250$ in central Au+Au at $\sqrt{s} = 130$AGeV at midrapidity. We will employ $s/\rho_B = 200$ and dN_B/dy=25. The resulting baryon density at midrapidity is $\rho_i = 2.3\rho_0$. Hadron multiplicity ratios at midrapidity can be described with these initial conditions [44]. The energy density and baryon density are initially distributed in the transverse plane according to a so-called "wounded nucleon" distribution with transverse radius $R_T = 6$ fm. For further details, we refer to refs. [14, 20]. As seen from table II, the initial energy density more than doubles when going from CERN-SPS energy to BNL-RHIC energy. The initial temperature increases by about 50 MeV, while the initial chemical potential for u, d quarks decreases by about 100 MeV, in all cases. Note that for a bag model EoS the chemical potential for s-quarks vanishes because of strangeness neutrality in the QGP phase, see e.g. [14]. Strangeness neutrality is a global constraint, only

[26]. Within a mixed phase, however, the individual phases may adopt non-zero values for f_s. In a hadronic model, the hyperons contain non-strange quarks and adopt a finite chemical potential if $\mu_q \neq 0$. Therefore, the hyperon vector density is positive at finite temperature. This surplus of strange quarks contained in the hyperons is balanced by the anti-strange quarks in strange mesons. This leads to a finite strangeness chemical potential μ_s, which is adjusted to yield $n_s = n_{\bar{s}}$. Here $n_s, n_{\bar{s}}$ denote the total number of strange and anti-strange quarks in the system, respectively. As already discussed in [26], in the mixed phase only the total strangeness fraction f_s vanishes, while each of the two coexisting phases does, in general, carry net strangeness. Furthermore for the case of a strong first order phase transition the evaporation of pions and kaons and strangeness distillation [26] should be studied, since these influence the unlike particle correlations (e.g. K^+/K^-, see [27]).

3. RESULTS

3.1. Hypersurfaces

Before presenting results on pion correlations, in this section we shall discuss the effects from varying the latent heat in the EoS on the space-time evolution of the hadronic fluid. Qualitatively, the same effects are observed for both sets of initial conditions, and we therefore show only the results corresponding to the BNL-RHIC case. Figure 4 shows the calculated hypersurfaces at fixed temperature, $T = T_f$, in the transverse plane at $\eta = 0$ for the three chiral EoS.

Comparing the freeze-out curves for the different equations of state one finds that the different phase-transition behavior of the three parameter sets is reflected in the space-time evolution of the system. In case I (crossover) the time until freeze-out is shorter than in case III (two first order phase transitions). This is not surprising, since the occurence of a mixed phase prolongs the expansion time. This is due to the above-mentioned drop of the speed of sound, c_s. The fastest expansion is obtained for a crossover with no latent heat and, accordingly, no discontinuity in the entropy density.

The different space-time evolutions for the three EoS is most obvious for $T_f = 80$MeV and $T_f = 100$MeV but can also be seen for $T_f = 130$MeV. For CERN-SPS energies we obtained similar results, with only slightly smaller liefetimes and radial extensions.

3.2. Two particle correlations

To calculate the two particle correlation function we use the method developed in [4, 8]. We measure the coincidence probability $P(\mathbf{p_1}, \mathbf{p_2})$ of two identical particles with momenta $\mathbf{p_1}, \mathbf{p_2}$ relative to the probability of detecting uncorrelated particles. The inverse width of the correlation function in out-direction (R_{out}) is proportional to the duration of the particle emission, i.e. to the lifetime of the source [8, 38]. Analogously, the inverse width of the correlation function in side-direction (R_{side}) is a measure for the (transverse) size of the source. Using a Gaussian fit one can relate the inverse widths of the correlation functions to radius parameters. It was pointed out in [10] that both for model calculation as well as for experimental data it is tedious, if not impossible, to relate R_{side} and R_{out} to the real source size and lifetime. However, the ratio R_{out}/R_{side} can be used as a measure for the lifetime of the system.

The HBT radii shown below are obtained as follows. We assume that the pion correlation function is determined on a hypersurface of given temperature T_f, where the pion mean free path supposedly becomes too large to maintain local equilibrium. As already mentioned above, at present we refrain from a detailed study of transport coefficients of our model. Rather, our approach shall be more pragmatic, and we shall consider T_f as a free parameter.

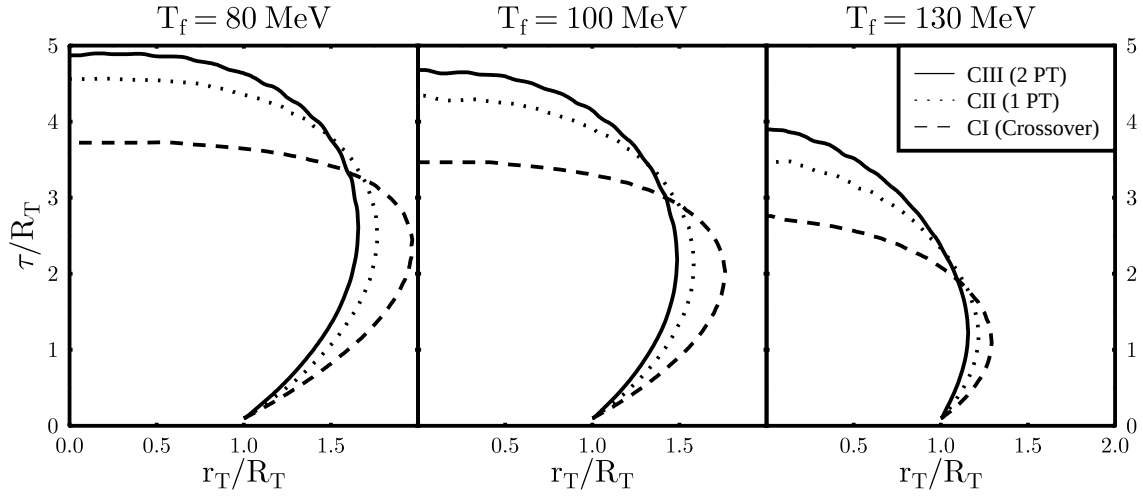

FIG. 4: Hypersurfaces $T = T_f$ for the three chiral EoS. This figure corresponds to initial conditions as appropriate for central Au+Au collisions at BNL-RHIC energy ($\sqrt{s} = 130$AGeV).

On the $T = T_f$ hypersurface, the two-particle correlation function is given by [9, 10]

$$C_2(\mathbf{p}_1, \mathbf{p}_2) = 1 + \frac{1}{\mathcal{N}} \left| \int \mathrm{d}\sigma \cdot K e^{i\sigma \cdot q} f\left(u \cdot K/T\right) \right|^2 \tag{4}$$

The normalization factor $\mathcal{N}$ is given by the product of the invariant single-particle inclusive distributions of the pions evaluated at momenta $\mathbf{p}_1$ and $\mathbf{p}_2$, respectively. u^μ denotes the four-velocity of the fluid on the $T = T_f$ surface, σ^μ; $K^\mu = (p_1^\mu + p_2^\mu)/2$, $q^\mu = p_1^\mu - p_2^\mu$ are the average four-momentum and the relative four-momentum of the pion pair, respectively. For midrapidity pions, $K_\parallel = q_\parallel = 0$. Thus, for the cylindrical geometry, the correlation function depends on three variables only; that is, the *out* and *side* components of q, and the transverse momentum of the pion pair, K_T. In (4), f denotes the local distribution function of pions in momentum space, at a temperature T_f. For simplicity, we shall assume a thermal distribution function and neglect the interaction energy of the pions, which amounts to only a $\sim 5\%$ correction relative to the vacuum mass of the pion. From $C_2(q_{out}, q_{side}, K_T)$ we determine the HBT radii as $R_{\rm out} = \sqrt{\ln 2}/q^*_{\rm out}$ and $R_{\rm side} = \sqrt{\ln 2}/q^*_{\rm side}$, where $q^*_{\rm out}$, $q^*_{\rm side}$ are defined by $C_2(q^*_{\rm out}, q_{\rm side} = 0) = C_2(q^*_{\rm side}, q_{\rm out} = 0) = 3/2$.

In Fig. 5 we show the resulting HBT-radii R_{side} and R_{out} for central Pb+Pb collisions at SPS energy ($\sqrt{s}/A = 17.4$ GeV), and compare to recent preliminary data obtained by the NA49 collaboration [35]. Of course, in view of the approximations mentioned above such a comparison should be interpreted with care. At $T_f = 130$ MeV, R_{out} is reproduced reasonably well. In particular, it appears that the EoS with the largest latent heat overestimates R_{out}. This is rather similar to the bag model EoS [10, 20]. Note that R_{out} describes the size of the source folded with the mean emission duration [7, 8, 9, 10, 20, 38]. The average radius of the pion source decreases with increasing latent heat, but the emission duration increases. Integrating over the emission surface, Fig. 5 shows that for $K_T \geq 50$ MeV the latter dominates in case of longitudinal scaling expansion, and R_{out} increases with the latent heat of the chiral transition. The EoS with vanishing or small latent heat is closest to the data.

At $T_f = 80$ MeV and $T_f = 100$ MeV, the pion source has expanded further and hence R_{out} is larger. At large K_T, the EoS with first-order phase transition predicts too large values for R_{out} for both values of T_f. At small transverse momenta, on the other hand, all three EoS describe the data better than for the high freeze out temperature. This observation is in agreement with the results of ref. [20], which shows that due to dissipative effects particles

which suffer soft hadronic rescatterings freeze out at much later times than particles subject to harder interactions. We can not account for that effect within our ideal-fluid model, but it can be mimicked by choosing a lower T_f at smaller K_T. In any case, our main focus is on effects from the chiral phase transition. Our results suggest that a weakly first-order transition, or a smooth crossover, can give a better description of R_{out} than a phase transition with large latent heat (as in the bag model).

R_{side} measures the geometric size of the pion source in the transverse plane [46], and does not depend on the emission duration [7, 8, 9, 10, 20, 38]. First, we note that the effective source radius depends only very weakly on the latent heat for the transition, in particular for large T_f. This is in accord with the space-time evolution as described in 3.1. At small K_T, R_{side} decreases slightly with the latent heat. However, for all three EoS, R_{side} comes out too small. Only for $T_f = 80$ MeV an reasonable description is obtained. This could be partly due to the neglect of resonance decays, which form a "halo" surrounding the direct pion source [7, 9, 37, 39], and increase its effective size. On the other hand, the resonance decays would also tend to increase R_{out}. As discussed in [10], a reasonable measure for the

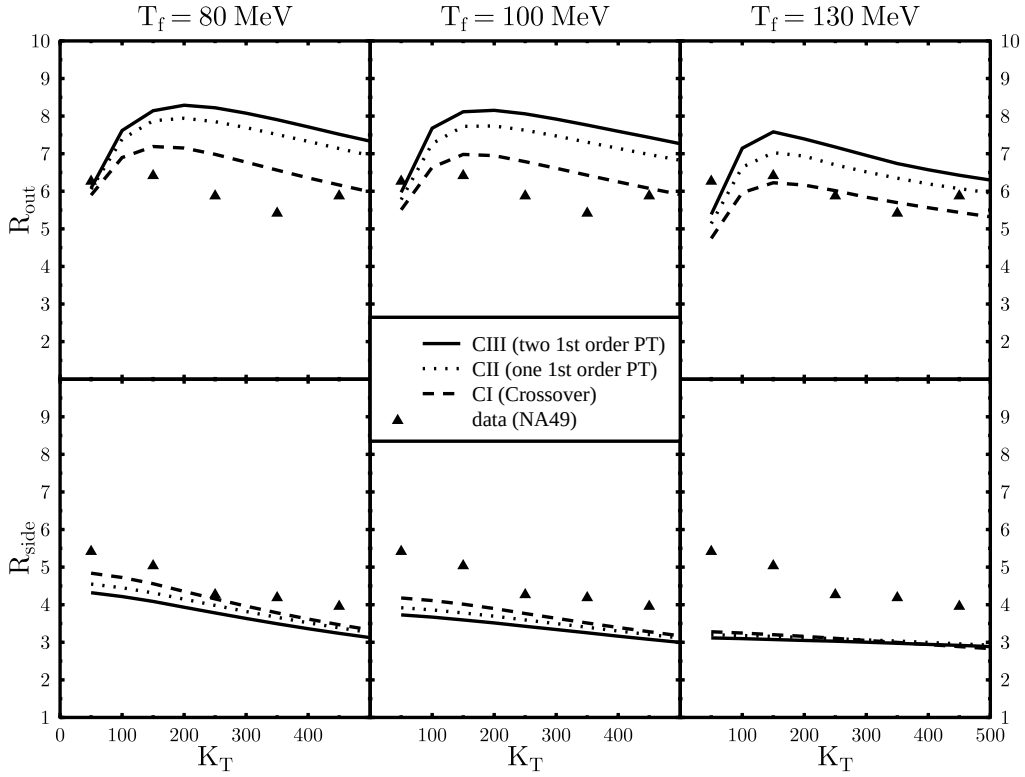

FIG. 5: R_{side} and R_{out} as a function of K_T at SPS. $T_f = 80, 100, 130$MeV.

emission duration of pions therefore is the ratio R_{out}/R_{side}, which is also less affected by resonance decays. In Fig. 6 we show the results for initial conditions appropriate for BNL-

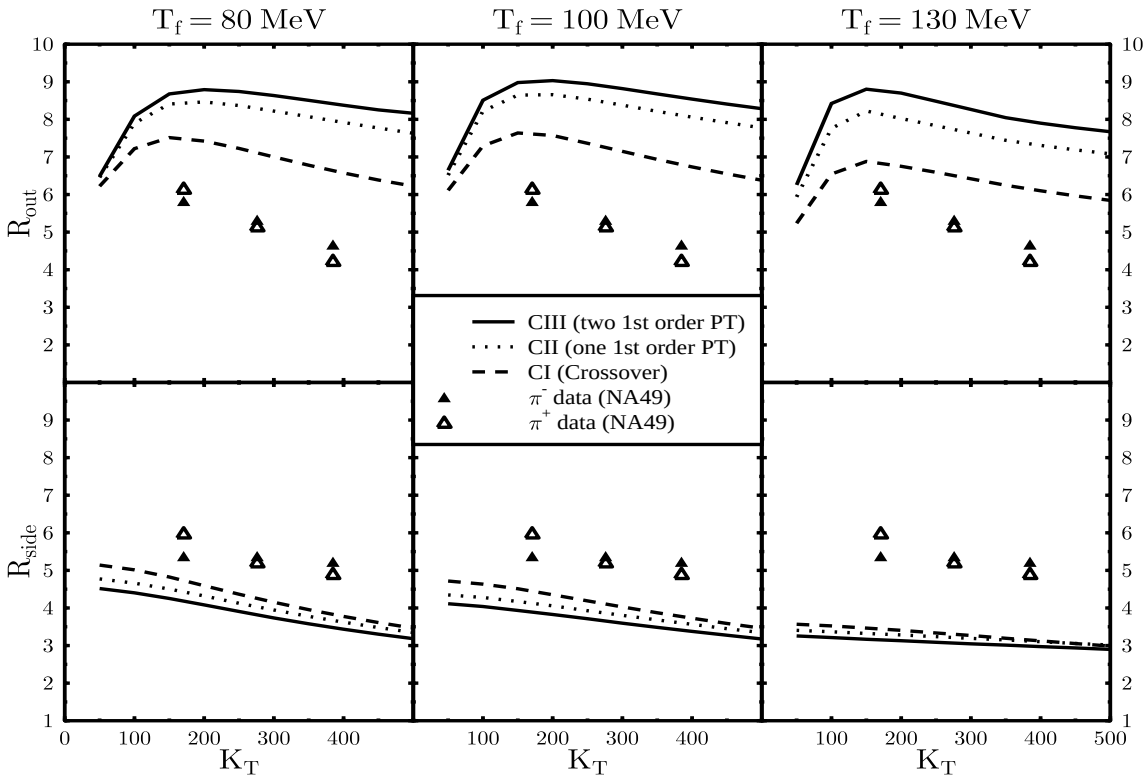

FIG. 6: R_{side} and R_{out} as a function of K_T at RHIC. $T_f = 80, 100, 130$MeV.

RHIC energies. Both radii increase as compared to the lower SPS energy. That is because the initial entropy density is significantly larger. Thus the system takes longer to cool down to T_f, and the system has more time to expand in the transverse direction. For example, at $K_T = 500$ MeV, R_{out} increases by about 1 fm for the EoS with a strongly first-order phase transition. R_{side} increases even less. This is in contrast to an EoS with only pions in the hadronic phase [8, 10, 38], where the ratio of entropies of the two thermodynamic phases is very large at T_c. The very moderate increase of the radii from SPS to RHIC energy is in agreement with the results from STAR for Au+Au collisions at RHIC [40]. On the other hand, as already discussed above, the "geometric size" of the source, R_{side}, is too small. As at SPS energy, this could be due to decays of resonances. We shall therefore discuss next the behavior of the ratio R_{out}/R_{side} with K_T, which is less affected by decays [10], and which is a good measure for the lifetime of the pion source.

Figures 7 and 8 show the experimentally measured ratio R_{out}/R_{side} as a function of K_T

for the three different equations of state for SPS and RHIC energies. One observes that at

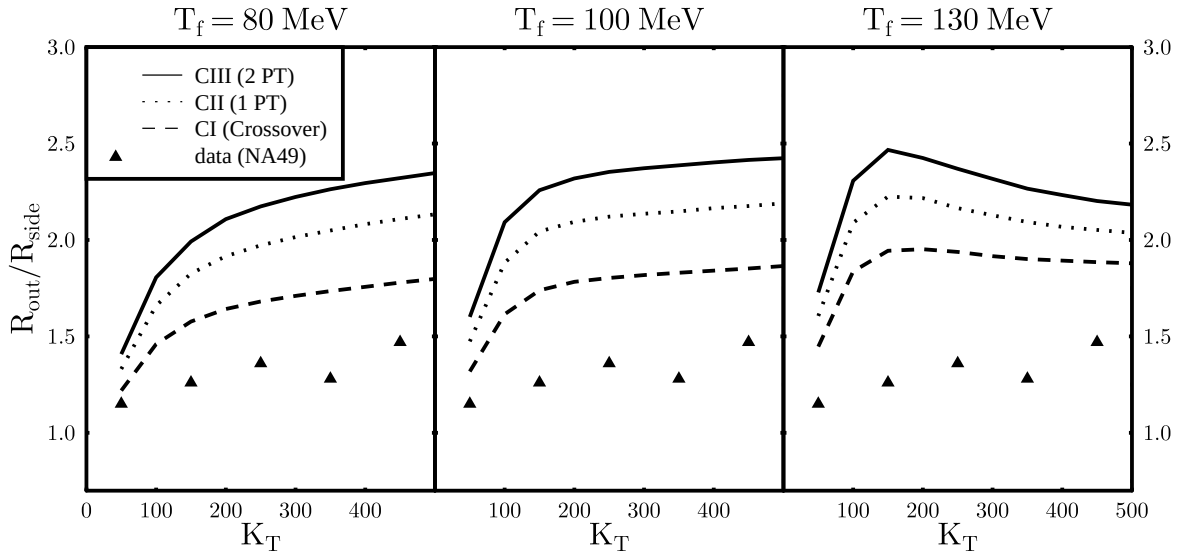

FIG. 7: R_{out}/R_{side} as a function of K_T at SPS.

both energies the shortest lifetime of the system emerges from the EoS featuring a crossover (CI), while the slowest expansion results from the EoS with largest latent heat (CIII). At SPS energy, the data [35] yield a slowly rising R_{out}/R_{side} ratio. This is obtained for all three EoS, if the freeze-out temperature is low, $T_f = 80, 100$ MeV. Of course, the absolute value of R_{out} is too large, while R_{side} is too small, and so the ratio comes out way too large. As is obvious from the figures, we are not able to reproduce the data for R_{out}/R_{side}, though a small or even vanishing latent heat and a smaller freeze-out temperature improve the picture. Turning to RHIC, we see that the predicted general behavior of R_{out}/R_{side} is similar as at the SPS, except for a slight overall increase of that ratio. That is because the larger initial entropy per baryon, which is deduced from the larger π/p and $\bar{p}/p$ ratios, increases the lifetime of the system slightly. On the other hand, the STAR data [40] show $R_{out}/R_{side} \simeq 1$, and a decrease with K_T. This behavior can evidently not be reproduced for low T_f. Larger freeze-out temperatures, $T_f = 130$ MeV, lead to flat, or even slightly decreasing R_{out}/R_{side}. Nevertheless, R_{out}/R_{side} is about a factor of 2 higher for $K_T \geq 100$ MeV than seen in the STAR data.

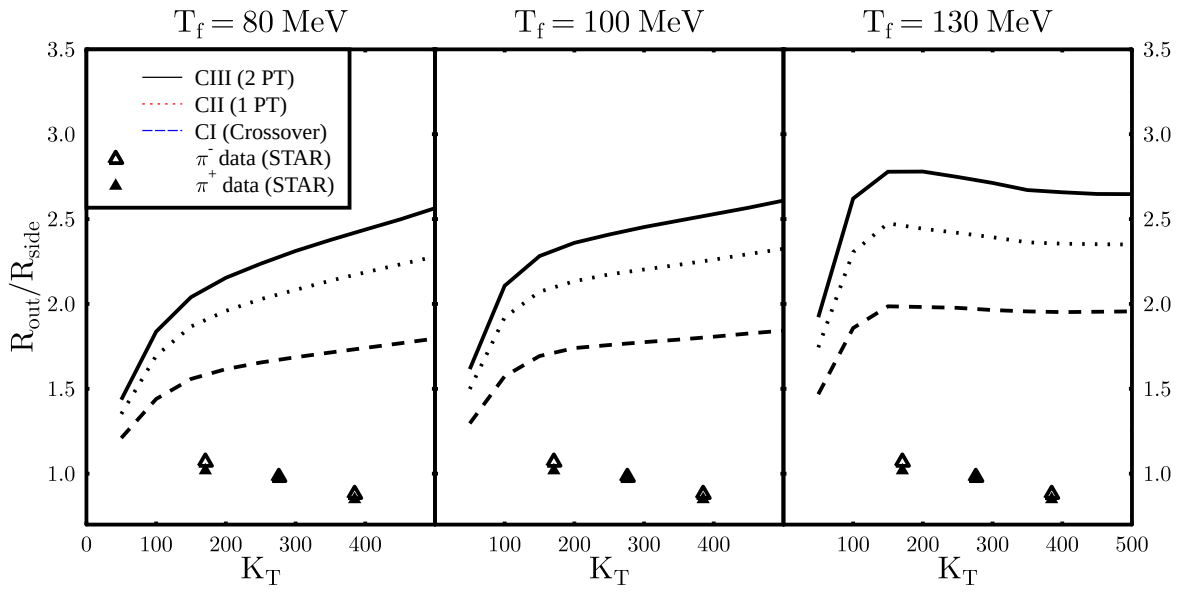

FIG. 8: R_{out}/R_{side} as a function of K_T at RHIC.

4. CONCLUSION

The space-time evolution of ultra-realtivistic heavy ion collisions at SPS and RHIC energies has been studied within hydrodynamic simulations using various EoS obtained from a chiral $SU(3) \times SU(3)$ model. HBT radii have been calculated and compared to data from the NA49 collaboration and the STAR collaboration. The influence of different orders of the chiral phase transition and the underlying EoS have been discussed.

A small latent heat, i.e. a weak first-order chiral phase transition or even a smooth crossover, leads to larger emission regions and smaller emission duration, as well as to larger R_{side} and smaller R_{out} HBT radii than a strong first order transition as for example assumed in the bag model.

In almost all cases, we observe that the results obtained with a crossover EoS are closest to the experimental data. However, a quantitative description of the data, both at SPS energy as well as at RHIC energy, is not possible within our present ideal-fluid approach with longitudinal scaling flow, employing the various SU(3) chiral EoS.

Apparently, conclusions can only be drawn after considerable improvements on various aspects of the description of high-energy heavy-ion collisions.

In particular, the effective chiral-SU(3) potential is rather rapidly varying around T_c. Therefore, a non-equilibrium description, accounting for supercooling effects and/or rapid spinodal decomposition, might be in order [25, 28]. In fact, it has been argued that the decay of a droplet of chirally symmetric matter from a region of negative pressure may

yield smaller values for the HBT radii, as well as a smaller ratio R_{out}/R_{side} [41][47]. Such considerations are out of the scope of the present manuscript but will be studied in detail in the future. More realistic freeze-out descriptions [20, 45] may improve the results. However, as dissipative effects are expected to prolong the lifetime of the pion source even more, it appears very likely that a quasi-adiabatic first-order phase transition with large latent heat, for which a hydrodynamic description should be adequate, can not describe the pion HBT data from CERN-SPS and from BNL-RHIC. This observation may be viewed as an experimental confirmation of the predictions from lattice QCD [2, 22], which do not show a large latent heat.

The nature of the chiral symmetry restoration will be better understood by analyzing forthcoming experimental data from RHIC. For example, correlations among kaons, protons, and non-identical particles can be analysed [42]. Excitation functions between CERN-SPS energy ($\sqrt{s} = 17.4A$ GeV) and the present BNL-RHIC energy ($\sqrt{s} = 130 - 200$ AGeV) would be extremely useful to provide a more detailed view of the behavior of the correlation functions. The excitation functions of source sizes and lifetimes and also so-called "azimuthally sensitive" HBT-analysis [43] could be useful to obtain a complete picture of the phase transition via the structure of the pion source in space-time. With these data emerging, we hope that it will be possible to obtain a deeper understanding of the QCD phase transition in high-energy heavy-ion collisions.

Acknowledgement

We would like to thank A. Dumitru and D. Rischke for numerous discussions and for providing the relativistic hydrodynamics and the appropriate correlation function codes. We also thank K. Bugaev, I. Mishustin and L. Satarov for discussions. This work was supported by Deutsche Forschungsgemeinschaft (DFG), Gesellschaft für Schwerionenforschung (GSI), Bundesministerium für Bildung und Forschung (BMBF), Graduiertenkolleg Theoretische und experimentelle Schwerionenphysik and by the U.S. Department of Energy, Nuclear Physics Division (Contract No. W-31-109-Eng-38).

---

[1] R. D. Pisarski and F. Wilczek, Phys. Rev. D **29**, 338 (1984).

[2] F. R. Brown *et* al., Phys. Rev. Lett. **65**, 2491 (1990); Y. Iwasaki, K. Kanaya, S. Kaya, S. Sakai and T. Yoshie, Z. Phys. C **71**, 343 (1996).

[3] G. Goldhaber, S. Goldhaber, W. Lee and A. Pais, Phys. Rev. **120**, 300 (1960).

[4] E. Shuryak, Phys. Lett. **B44**, 387 (1973); M. Gyulassy, S. K. Kauffmann and L. W. Wilson, Phys. Rev. **C20**, 2267 (1979); A. Makhlin and Y. Sinyukov, Z. Phys. **C39**, 69 (1988); Y. Hama and S. S. Padula, Phys. Rev. **D 37**, 3237 (1988).

[5] K. Kajantie and L. McLerran, Ann. Rev. Nucl. Part. Sci. **37**, 293 (1987); J. W. Harris and B. Müller, Ann. Rev. Nucl. Part. Sci. **46**, 71 (1996); S. A. Bass, M. Gyulassy, H. Stöcker and W. Greiner, J. Phys. G **G25**, R1 (1999).

[6] R. M. Weiner, Phys. Rept. **327**, 249 (2000); T. Csörgő, hep-ph/0001233.

[7] U. Wiedemann and U. Heinz, Phys. Rept. **319**, 145 (1999).

[8] S. Pratt, Phys. Rev. **D33**, 1314 (1986); G. Bertsch, M. Gong, M. Tohyama, Phys. Rev. **C37**, 1896 (1988); G. Bertsch, Nucl. Phys. **A498**, 173c (1989).

[9] B. R. Schlei, U. Ornik, M. Plümer and R. M. Weiner, Phys. Lett. **B293**, 275 (1992); J. Bolz, U. Ornik, M. Plümer, B. R. Schlei and R. M. Weiner, Phys. Rev. **D47**, 3860 (1993); Phys. Lett. **B300**, 404 (1993).

[10] D.H. Rischke and M. Gyulassy, Nucl. Phys. **A608**, 479 (1996)

[11] L.D. Landau and E.M. Lifshitz, "Fluid Mechanics", Pergamon Press, New York, 1959

[12] K. Kajantie and L. McLerran, Phys. Lett. B **119**, 203 (1982); Nucl. Phys. **B214**, 261 (1983); J.D. Bjorken, Phys. Rev. D **27**, 140 (1983); G. Baym, B.L. Friman, J.P. Blaizot, M. Soyeur, and W. Czyz, Nucl. Phys. **A407**, 541 (1983); K. Kajantie, R. Raitio, and P.V. Ruuskanen, Nucl. Phys. **B222**, 152 (1983)

[13] e.g. H. Stöcker *et* al., Phys. Rev. C **25**, 1873 (1982); Nucl. Phys. A **566**, 15C (1994); R. Venugopalan, M. Prakash, M. Kataja and P. V. Ruuskanen, Nucl. Phys. A **566**, 473C (1994); A. Dumitru, et al., Phys. Rev. C **51**, 2166 (1995); B. R. Schlei, U. Ornik, M. Plümer, D. Strottman and R. M. Weiner, Phys. Lett. B **376**, 212 (1996); J. Brachmann et al., Phys. Rev. C **61**, 024909 (2000); K. Morita, S. Muroya, H. Nakamura and C. Nonaka, Phys. Rev. C **61**, 034904 (2000).

[14] A. Dumitru and D. H. Rischke, Phys. Rev. C **59**, 354 (1999).

[15] D.H. Rischke, S. Bernard, and J.A. Maruhn, Nucl. Phys. **A595**, 346 (1995)

[16] D.H. Rischke and M. Gyulassy, Nucl. Phys. **A597**, 701 (1996)

[17] P. Papazoglou, D. Zschiesche, S. Schramm, J. Schaffner-Bielich, H. Stöcker, and W. Greiner, Phys. Rev. C **59**, 411 (1999).

[18] D. Zschiesche, P. Papazoglou, S. Schramm, C. Beckmann, J. Schaffner-Bielich, H. Stöcker, and W. Greiner, Springer Tracts in Modern Physics **163**, 129 (2000).

[19] H. A. Weldon, Z. Phys. **C54**, 431 (1992); M. Prakash, M. Prakash, R. Venugopalan and G. Welke, Phys. Rept. **227**, 321 (1993); K. Haglin and S. Pratt, Phys. Lett. **B328**, 255 (1994).

[20] S. Soff, S. A. Bass and A. Dumitru, Phys. Rev. Lett. **86**, 3981 (2001); S. A. Bass, A. Dumitru, M. Bleicher, L. Bravina, E. Zabrodin, H. Stöcker and W. Greiner, Phys. Rev. C **60**, 021902 (1999).

[21] A. Muronga, nucl-th/0104064.

[22] E. Laermann, Nucl. Phys. **A610**, 1c (1996)

[23] B. D. Serot and J. D. Walecka, Int. J. Mod. Phys. E **6**, 515 (1997)

[24] J. Theis, G. Graebner, G. Buchwald, J. A. Maruhn, W. Greiner, H. Stöcker and J. Polonyi, Phys. Rev. D **28** (1983) 2286.

[25] A. Chodos, F. Cooper, W. Mao and A. Singh, Phys. Rev. D **63**, 096010 (2001); O. Scavenius, A. Dumitru, E. S. Fraga, J. T. Lenaghan and A. D. Jackson, Phys. Rev. D **63**, 116003 (2001).

[26] C. Greiner, P. Koch and H. Stöcker, Phys. Rev. Lett. **58** (1987) 1825; C. Greiner, D. Rischke, H. Stöcker and P. Koch, Phys. Rev. D **38** (1988) 2797; C. Greiner and H. Stöcker, Phys. Rev. D **44** (1991) 3517; C. Spieles, H. Stöcker and C. Greiner, Eur. Phys. J. C **2** (1998) 351

[27] S. Soff, D. Ardouin, C. Spieles, S.A.Bass, H. Stöcker, D. Gourio, S. Schramm, C. Greiner, R. Lednicky, V.L. Lyuboshits, J.P. Coffin, C. Kuhn, J. Phys. G **23** (1997) 2095; D. Ardouin *et* al., Phys. Lett. B **446** (1999) 191.

[28] A. Dumitru and R. D. Pisarski, Phys. Lett. B **504** (2001) 282; O. Scavenius, A. Dumitru and A. D. Jackson, Phys. Rev. Lett. **87** (2001) 182302

[29] A. Chodos, R.L. Jaffe, K. Johnson, C.B. Thorn, and V.F. Weisskopf, Phys. Rev. D **9**, 3471 (1974)

[30] J. Letessier, A. Tounsi, U. Heinz, J. Sollfrank and J. Rafelski, Phys. Rev. Lett. **70**, 3530 (1993); P. Braun-Munzinger, I. Heppe and J. Stachel, Phys. Lett. B **465**, 15 (1999); D. Zschiesche, P. Papazoglou, C. W. Beckmann, S. Schramm, J. Schaffner-Bielich, H. Stöcker and W. Greiner, Nucl. Phys. A **663**, 737 (2000).

[31] K. Geiger and J.I. Kapusta, Phys. Rev. D **47**, 4905 (1993)

[32] T. Schönfeld, H. Stöcker, W. Greiner, and H. Sorge, Mod. Phys. Lett. A **8**, 2631 (1993)

[33] H. Stöcker et al., in Proc. 4th Int. Workshop "Relativ. Aspects of Nucl. Phys.", Rio de Janeiro 1995 (Brazil) (eds. T. Kodama, K.C. Chung, Y. Hama, G. Odyniec, H. Ströbele, C.-Y. Wong), World Scientific, Singapore, 1996, p. 437

[34] S. E. Vance, M. Gyulassy and X. N. Wang, Nucl. Phys. A **638** (1998) 395C [nucl-th/9802036].

[35] C. Blume, talk given at Quark Matter 2001, Jan. 15–20, Stony Brook, NY, USA.

[36] A. Makhlin and Y. Sinyukov, Z. Phys. **C39**, 69 (1988); Y. Hama and S. S. Padula, Phys. Rev. **D 37**, 3237 (1988).

[37] T. Csörgő, B. Lörstad and J. Zimanyi, Z. Phys. C **71**, 491 (1996).

[38] S. Pratt, Phys. Rev. Lett. **53**, 1219 (1984); Phys. Rev. **C49**, 2722 (1994).

[39] M. Gyulassy and S. S. Padula, Phys. Lett. B **217** (1989) 181.

[40] C. Adler *et* al. [STAR Collaboration], Phys. Rev. Lett. **87** (2001) 082301.

[41] T. Csörgő and L. P. Csernai, Phys. Lett. B **333**, 494 (1994).

[42] S. Panitkin, talk given at Quark Matter 2001, Jan. 15–20, Stony Brook, NY, USA; F. Retiere [CTAR Collaboration], nucl-ex/0111013.

[43] M. A. Lisa, U. Heinz and U. A. Wiedemann, Phys. Lett. B **489**, 287 (2000); M. A. Lisa *et* al. [E895 Collaboration], Phys. Lett. B **496**, 1 (2000); nucl-ex/0104012.

[44] N. Xu and M. Kaneta, nucl-ex/0104021; P. Braun-Munzinger, D. Magestro, K. Redlich and J. Stachel, hep-ph/0105229.

[45] K. A. Bugaev, Nucl. Phys. A **606**, 559 (1996); V. K. Magas *et* al., Heavy Ion Phys. **9**, 193 (1999); C. Anderlik *et* al., Phys. Rev. C **59**, 3309 (1999).

[46] More precisely, it corresponds to the scale of spatial homogeneity [36].

[47] Note, however, that within our effective theory for chiral symmetry restoration the spinodal instability occurs before negative pressure is reached, see Fig. 3.